Journal of Alloys and Compounds 508 (2010) 99–105

Contents lists available at ScienceDirect

Journal of Alloys and Compounds

journal homepage: www.elsevier.com/locate/jallcom

Simple preparation of sub-micron mesoporous TiO_2 spheres consisting of anatase nanocrystals

Sheng Li[a], Qianhong Shen[a,b,*], Jianjuan Zong[b], Hui Yang[a,b,**]

[a] Department of Materials Science and Engineering, Zhejiang University, Hangzhou 310027, PR China
[b] Zhejiang California International NanoSystems Institute, Hangzhou 310029, PR China

ARTICLE INFO

Article history:
Received 17 March 2010
Received in revised form 29 April 2010
Accepted 30 April 2010
Available online 6 May 2010

Keywords:
Nanostructured materials
Crystal growth
Catalysis
Microstructure

ABSTRACT

Mesoporous anatase titania spheres with an average size of approx. 400 nm were facilely prepared at low temperature by treating the titanium glycolate precursor spheres with hot water (~100 °C). The surface of the precursor particle became rough and the anatase phase began to form when it was treated with hot water for 1.5 h. With increasing treatment time, the crystallinity of the particles was improved, and the nanoporous structure further formed in the interior of the spheres. When the treatment time was prolonged to 6 h, the mesoporous anatase spheres were finally obtained, and they were composed of interconnected nanocrystals with the size less than 15 nm and pores with the mean size of 8.31 nm. The as-prepared mesoporous anatase titania spheres exhibited excellent adsorption capacity and better photocatalytic activity compared with the commercial photocatalyst P-25 due to the large specific surface area. Ostwald ripening and surface energy effects were presumed to play an important role in the formation of mesoporous structure and anatase nanocrystals.

1. Introduction

Titanium dioxide (TiO_2) currently has become one of the most popular semiconductor photocatalysts due to its low-cost, non-toxicity, chemical inertness and photostability. It has been widely used in many fields such as energy conversion, environmental remediation, biomedicine engineering and sensor [1–3]. Although nanosized TiO_2 powder usually exhibits a high photocatalytic activity, it is hard to separate and reuse this kind of powder from the aqueous suspensions, thus limiting its practical application. The immobilization of the TiO_2 catalysts on some supporting materials such as glass, Si, or indium tin oxides (ITO) substrates has been frequently adopted to overcome this problem [4,5]. However, the photocatalytic efficiency is often weakened owing to the huge loss in the contact area with the light source and reactant [6]. Fortunately, large size porous TiO_2 powder consisting of nanoparticles is able to resolve the difficulty of recycling to some extent [7]. Besides, porous TiO_2 with a large surface area can adsorb more O_2 and H_2O which are the reaction source of active groups, exhibiting higher photocatalytic activity. Meanwhile, the catalytic rate can be also accelerated as the porous powder is able to adsorb more reactants on the surface and increase the contact area. As is well known, the anatase phase shows the greatest activity among the several crystalline phases of titania. Hence, the large scale porous anatase TiO_2 powder is expected to be the new generation photocatalyst because of the high photocatalytic activity and easy recovery.

Many different kinds of methods have been reported to synthesize porous titania materials. The most common approach is template-based method which relies on soft templates (*e.g.* block copolymers and supra molecular assemblies of surfactants) [8–11] and hard templates (*e.g.* porous alumina, silica and polystyrene spheres, *etc.*) [12,13]. For the organic templates, high temperature thermal treatment (over 400 °C) or hydrothermal treatment is usually adopted to remove them, meanwhile accompanied with the crystallization of amorphous TiO_2 [8,9]. Certainly, the templates can also be extracted by organic solvent (*e.g.* anhydrous ethanol and toluene), mild acid or alkali treatment at low temperature [10–13]. However, the thermal treatment processes frequently lead to the partial or total collapse of the porous structure. Moreover, some templates cannot be eliminated completely by either calcination or solvent extraction sometimes [14]. Thus, the performance and application of porous titania materials may be restricted to a certain extent. Some other fabrication strategies are also reported. Kotani et al. used hot water treatment process to leach the poly (ethylene glycol) (PEG) in the TiO_2–SiO_2 thin films out in less than one minute and made the film porous. This treatment also led to the formation of anatase nanocrystals in the whole film. But they concluded that it is a unique phenomenon in the present SiO_2–TiO_2 system, and ascribed the nucleation of anatase nanocrystals to the hydrolysis

* Corresponding author.
** Corresponding author. Tel.: +86 571 87951408; fax: +86 571 87953054.
E-mail addresses: s_qianhong@163.com (Q. Shen), yanghui@zju.edu.cn (H. Yang).

0925-8388/$ – see front matter © 2010 Elsevier B.V. All rights reserved.
doi:10.1016/j.jallcom.2010.04.246

of Si–O–Ti bonds [15,16]. In contrast to template-based method, only a few studies involved the synthesis of porous titania without assisting of templates [17–19].

In this paper, sub-micron-sized mesoporous TiO_2 spheres consisting of anatase nanocrystals were synthesized by simply treating the titanium glycolate precursor spheres with hot water (~100 °C) in the absence of templates. The changes in morphology, microstructure and composition of the precursor particles with hot water or high temperature thermal treatment for different times were compared, and the photocatalytic activity of different products was also investigated using Rhodamine-B (RhB) as a photocatalytic reactant. Probable mechanisms for the simultaneous formation of porous structure and anatase nanocrystals were discussed in detail.

2. Experimental

2.1. Preparation of TiO_2 precursor spheres

The monodisperse titanium glycolate precursor spheres were prepared according to the reference with some modifications [20]. In a typical synthesis, 5 g tetrabutoxytitanium (TBT, 98%) was added to 50 g ethylene glycol (EG, AR) in a sealed conical flask. The solution was magnetically stirred for 10 h at room temperature, then the glycolated precursor was immediately poured into acetone (99.5%) containing ~0.3% water at the molar concentration of 91 mM (calculated as the final concentration of the precursor in acetone) under vigorous stirring for 20 min and then aging for ~30 min. The white precipitate was harvested by centrifugation, followed by washing with ethanol and deionized water several times to remove EG from the surfaces of the titania glycolate particles and was dried at 50 °C for further usage.

2.2. Fabrication of mesoporous TiO_2 particles

0.5 g TiO_2 precursor spheres were redispersed in 100 g deionized water followed by ultrasonic vibration for 15 min to attain a better dispersion, and the solution was refluxed at the boiling point (~100 °C) under slightly stirring for different periods. The white precipitate was recovered by centrifugation, then washed with deionized water and ethanol several times, and dried at 50 °C for further usage. The final mesoporous TiO_2 products were named as MT-*x* (here, *x* is an arabic number representing the treatment time (min)). Besides, compact TiO_2 spheres prepared by thermal treatment at 500 °C for 2 h (named as CT-500) were also used as reference.

2.3. Characterization

The morphology and microstructure changes of the TiO_2 spherical particles were examined using field-emission type transmission electron microscope (TEM, JEOL JEM-1230), high-resolution transmission electron microscope (HRTEM, PHILIPS CM200) and scanning electron microscope (FE-SEM, FEI SIRION-100). Crystallinity of the powders was examined from the X-ray diffraction (XRD) patterns using a PANalytical's X'Pert PRO diffractometer (CuKα, 40 kV, 40 mA) for 2θ in the range from 20° to 80°. The average crystallite size of anatase was calculated according to the Scherrer's formula using the fwhm (full width at half-maximum) data of the major diffraction peak (1 0 1), and the instrumental line broadening was corrected by using silicon as a standard. N_2 adsorption measurements were performed on a Micromeritics ASAP 2020 apparatus at 77 K. The specific surface area of the samples was calculated by using the multiple-point Brunauer–Emmett–Teller (BET) method in the relative pressure range $P/P_0 = 0.05–0.3$. The pore size distribution curves were computed by using the Barrett–Joyner–Halenda (BJH) method, and pore sizes were obtained from the peak positions of the distribution curves. Fourier transformed infrared (FTIR) spectra of the samples were acquired in air using a spectrophotometer (Thermo Nicolet 5700).

The photocatalytic properties of the different powders were evaluated using decomposition of RhB in a deionized water solution. P-25 powder was also adopted as the reference for comparison. 15 mg catalyst was added to 60 g RhB aqueous solution (with the concentration of 5 mg L^{-1}). The solution was completely adsorbed under closed light for 2 h at first, and then irradiated with a high-pressure Hg lamp (500 W) for different times. Changes in concentrations of RhB in the aqueous solution were examined from absorption spectra measured on a UV–vis-NIR spectrophotometer (HITACHI U-4100).

3. Results and discussion

3.1. Characterization of morphology and structure

Fig. 1a shows the SEM image of the monodisperse titanium glycolate precursor spheres (approx. 400 nm in diameter) with a good dispersivity. The bright field TEM image of the spherical colloids (Fig. 1b) indicates that the spherical particles have a rather compact structure and their surfaces are very smooth.

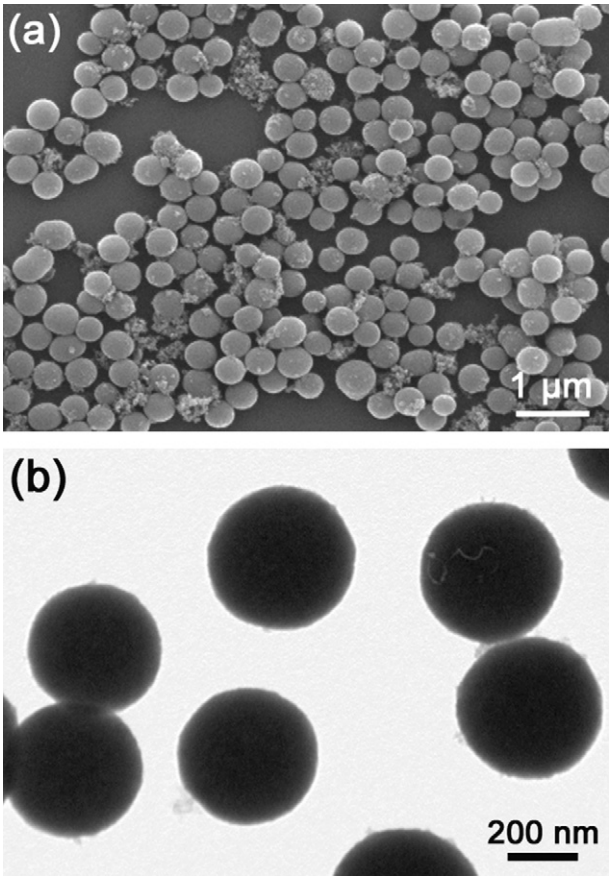

Fig. 1. SEM image (a) and TEM image (b) of the titanium glycolate precursor spheres.

Fig. 2 presents the XRD patterns of the titanium glycolate precursor spheres before and after hot water treatment for various times, and the sample CT-500 is also shown in the image for comparison. It is apparent that the TiO_2 precursor does not show any diffraction

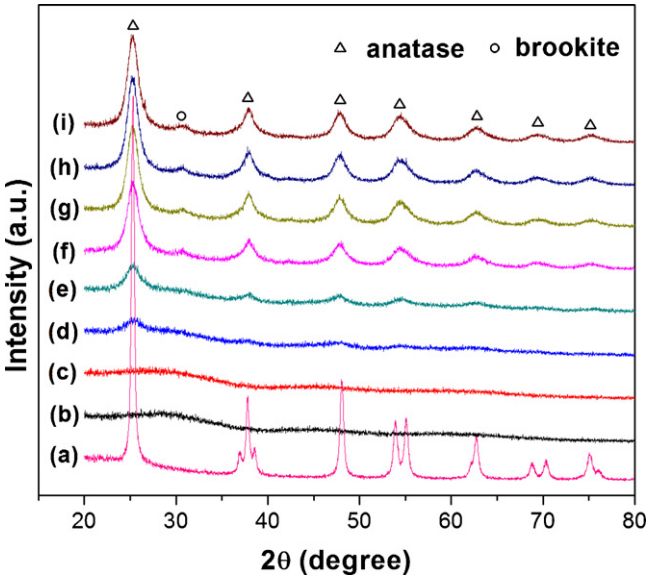

Fig. 2. X-ray diffraction patterns of (a) CT-500, (b) TiO_2 precursors, (c) MT-30, (d) MT-90, (e) MT-120, (f) MT-180, (g) MT-240, (h) MT-300 and (i) MT-360.

peak, suggesting its amorphous nature. After treating for 30 min, MT-30 is also almost amorphous. When the precursor is treated for 90 min, several diffraction peaks appear and all of them can be clearly attribute to the anatase phase (JCPDS No. 21-1272; space group, $I4_1/amd$ (141)) of TiO_2. With the increase of treatment time, the peak intensities of anatase increase, indicating the enhancement of crystallization. Meanwhile, the (1 0 1) plane diffraction peaks of anatase become sharper and sharper, showing the increase of anatase crystallite size. However, there is slight change in the intensity when the hot water treatment time exceeds 180 min, and further increase of treatment time has no obvious influence on the phase structures and composition of the samples. Besides, the weak peak at $2\theta = 30.7^\circ$ belonging to the brookite phase (JPCDS No. 29-1360; space group, *Pcab* (61)) is also detected. As observed, the sample CT-500 is made of pure anatase, and the anatase diffraction peaks of the powder obtained at low temperature are much broader than CT-500. It indicates that the size of anatase crystals in the TiO_2 particles formed by the hot water treatment is much smaller.

Typical TEM images of changes in morphology of the TiO_2 spherical particles with different treatment times are chosen and compared in Fig. 3. For MT-30 (Fig. 3a), there are very few fine clusters on the surface of the particles, thus the surface is almost smooth. When the treatment time is increased to 90 min (Fig. 3b), the surface of MT-90 spheres gets a little rough and begins to crystallize according to the results of XRD. The porous structure on the surface layer of the spheres is formed after treating for 180 min (Fig. 3c). With increasing reaction time to 300 min, the loose porous structure gets deeply into the interior of the MT-300 spheres (Fig. 3d). When the treatment time reached 360 min (Fig. 3e), the porous spheres consisting of interconnected TiO_2 nanoparticles and pores are finally obtained. In particular, the spherical morphology of these particles is nearly preserved. By contrast, the sample CT-500 (Fig. 3f) exhibits more compact structure and the mean diameter of colloids reduces by ~15% as a result of the phase transition from amorphous to anatase.

HRTEM studies were performed to further investigate the microstructure and crystallinity of MT-360. Fig. 4a shows a rep-

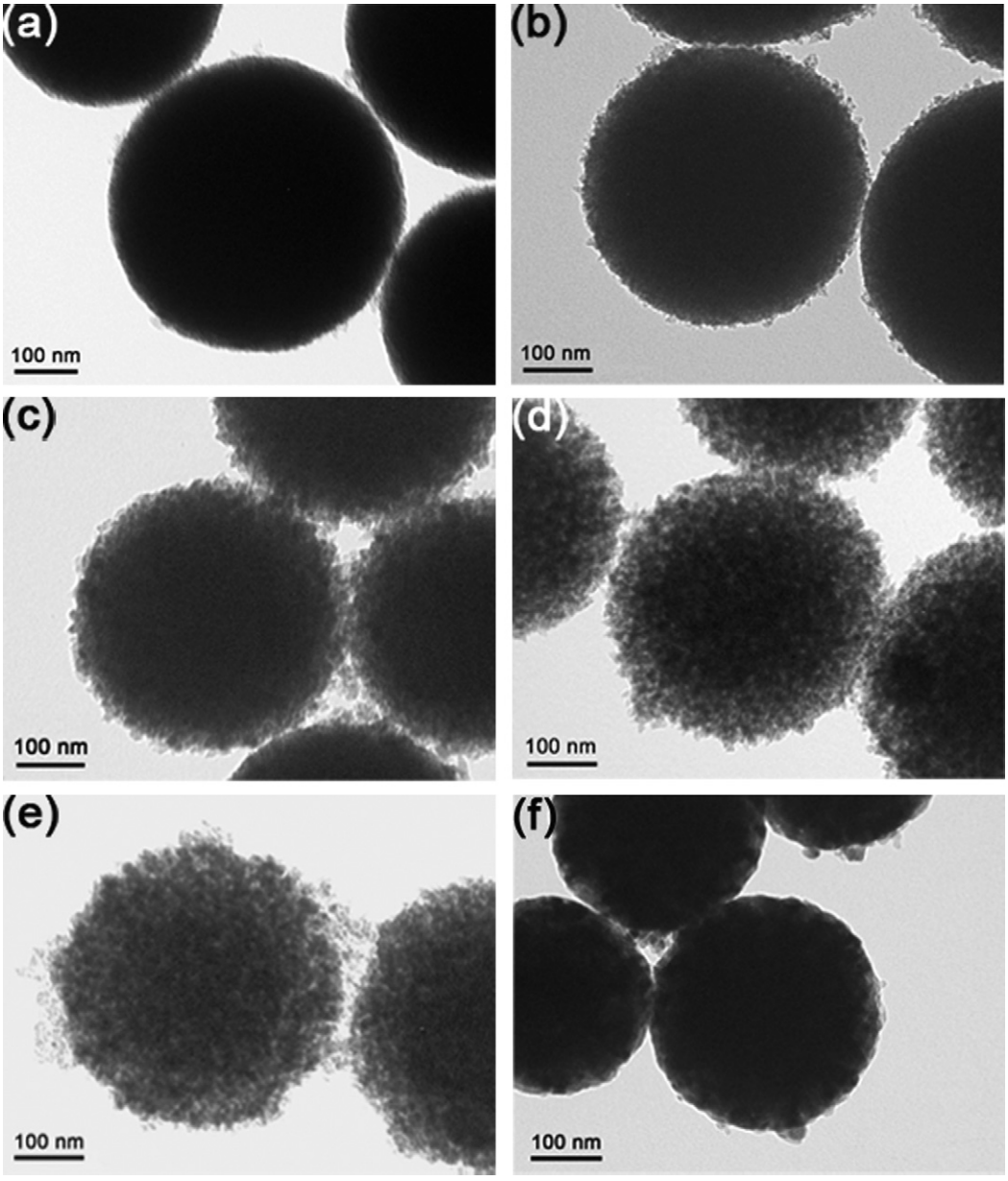

Fig. 3. TEM images of different spherical particles: (a) MT-30, (b) MT-90, (c) MT-180, (d) MT-300, (e) MT-360, and (f) CT-500.

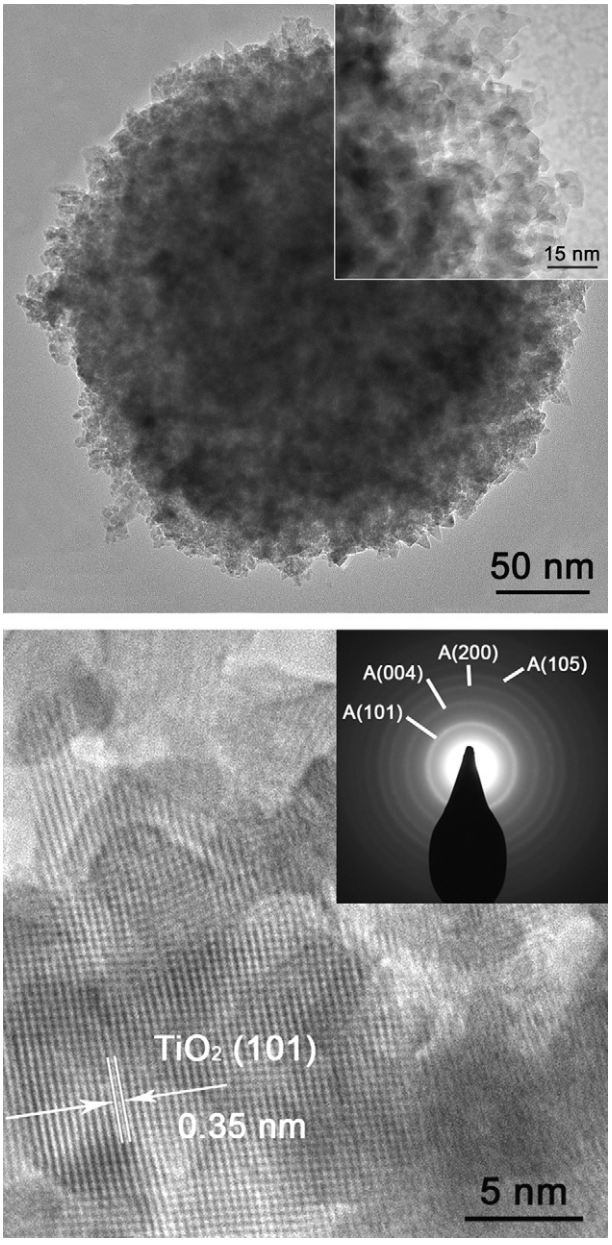

Fig. 4. HRTEM images of MT-360: (a) one typical mesoporous sphere, the inset is magnified image and (b) corresponding lattice fringes (with the electron diffraction pattern in the inset).

resentative HRTEM image of one TiO_2 mesoporous sphere with a magnified image in the inset. Compared to the compact structure of precursor spheres (Fig. 1b), the as-obtained TiO_2 spheres exhibit a hierarchically mesoporous structure. Further evidence of microstructure can be found from the inset image (Fig. 4a). It can be seen from the image that many nanocrystals with the size less than 15 nm and mesopores in size ranging from 2 nm to tens of nanometers are well dispersed in the sphere. Fig. 4b presents the corresponding HRTEM image of the same sample with the selected-area electron diffraction (SAED) pattern in the inset. The nanocrystals with a lattice fringe of 0.35 nm are attributed to the spacing of (1 0 1) in anatase TiO_2. In addition, the SAED pattern shows a set of diffraction rings which have been indexed to the (1 0 1), (0 0 4), (2 0 0), and (1 0 5) planes of the anatase phase, also revealing the formation of polycrystalline anatase phase.

Surface area and pore size distribution of the samples are determined by nitrogen adsorption measurements. Fig. 5 shows the

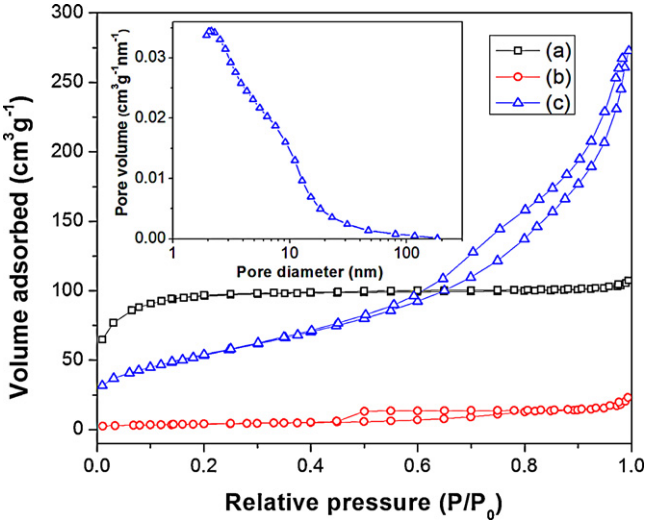

Fig. 5. Nitrogen adsorption and desorption isotherms of (a) precursor spheres, (b) CT-500, and (c) MT-360. Inset is the BJH pore size distribution curve of MT-360.

adsorption and desorption isotherms of the precursor spheres, CT-500 and MT-360, the inset is the BJH pore size distribution curve of MT-360. For the as-prepared amorphous TiO_2 and CT-500 samples, the isotherm is of type II (BDDT classification) which is the normal form of isotherm obtained with a non-porous adsorbent [21], and it is in accordance with the above TEM results. However, MT-360 exhibits a type IV isotherm curve (BDDT classification) with an H3 hysteresis loop at high relative pressure (P/P_0) between 0.6 and 1, indicating the presence of mesopores. The summary of the nitrogen adsorption–desorption results of above-mentioned products is listed in Table 1. After high temperature thermal treatment, the sample CT-500 shows a low BET specific surface area (14.21 $m^2\,g^{-1}$) owing to the large particle size and solid structure. While for the porous spheres treated by hot water, the BET specific surface area and pore volume reach 194.91 $m^2\,g^{-1}$ and 0.43 $cm^3\,g^{-1}$, respectively. According to the bulk density of anatase TiO_2 (1 g TiO_2 corresponds to a volume of 0.256 cm^3), the calculated porosity of the mesoporous spheres is 63%. Moreover, the pore sizes of porous spheres (inset of Fig. 5) mainly range from 2 nm to 15 nm. The average pore diameter is 8.31 nm, which is consistent with the above HRTEM results. However, the pore size is widely distributed. The larger pores may attribute to the aggregation of the particles. It is reported that the introduction of secondary larger pores could remarkably improve the activity of mesoporous catalysts due to the enhanced diffusion of reactants and products [22]. All of above results further support the fact that the sample after hot water treatment has a mesoporous structure.

3.2. Analysis of formation mechanism

Monodisperse titanium glycolate precursor spheres are synthesized through a homogeneous nucleation and growth process. When mixed with TBT, EG is sufficiently reactive to form glycolates

Table 1
Summary of the physical properties of different TiO_2 samples.

Sample	S_{BET}($m^2\,g^{-1}$)	Pore size (nm)	Pore volume ($cm^3\,g^{-1}$)	Crystallite size (nm)
Precursor	331.2	3.65	0.16	
MT-360	194.9	8.32	0.43	7.6
CT-500	14.2		0.03	24.0
P-25	51.0	3.80	0.06	30.0

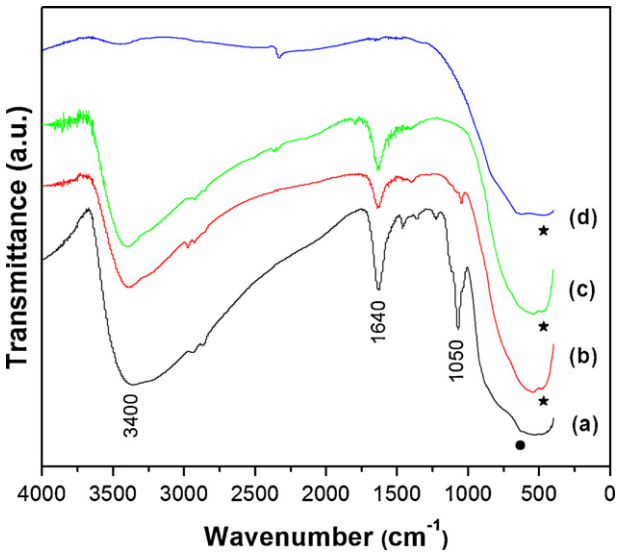

Fig. 6. FTIR spectra taken from (a) TiO_2 precursors, (b) MT-180, (c) MT-360 and (d) CT-500. Solid circle and asterisk denote the Ti–O stretching mode in the amorphous phase of titania (at ~640 cm^{-1}) and anatase phase (at ~465 cm^{-1}), respectively.

or mixed alkoxide/glycolate derivatives (see the reactions below): [20]

$$Ti(OBu)_4 + HOCH_2CH_2OH \rightarrow Ti(OCH_2CH_2O)(OBu)_2 + 2HOBu \quad (1)$$

$$Ti(OBu)_4 + 2HOCH_2CH_2OH \rightarrow Ti(OCH_2CH_2O)_2 + 4HOBu \quad (2)$$

Once the derivatives are poured into an acetone bath with a little water (~0.3%), the titanium glycolate precursor spheres are obtained, and they contain a lot of ethylene glycol units due to the partial hydrolysis and fast growth.

Fig. 6 shows FTIR spectra taken from the precursor and samples of MT-180, MT-360, and CT-500, respectively. The broad absorption peak appearing near 3400 cm^{-1} relates to a stretching vibration of Ti–OH group. At ~1640 cm^{-1}, a band corresponding to physically adsorbed water also appears. These results show that the hydroxyl group and surface adsorbed water are present in the products with hot water treatment. As the treatment time is increased, the peak corresponding to ethylene glycol units (the C–O stretching mode at ~1050 cm^{-1}) is reduced in intensity and then disappears. This peak is also not detected in the sample with thermal treatment. Ti–O stretching mode at ~640 cm^{-1} belonging to the amorphous structure shifts to ~465 cm^{-1} once the anatase phase is formed by hot water treatment or calcination. These observations are consistent with the reported literature [20]. All of the above results demonstrate that the porous anatase spheres are synthesized by the further hydrolysis and condensation process of the precursor, which can be expressed as follows:

$$Ti(OCH_2CH_2O)(OBu)_2 + 4H_2O \rightarrow Ti(OH)_4 + 2HOBu + HOCH_2CH_2OH \quad (3)$$

$$Ti(OCH_2CH_2O)_2 + 4H_2O \rightarrow Ti(OH)_4 + 2HOCH_2CH_2OH \quad (4)$$

$$Ti(OH)_4 \rightarrow TiO_2 \bullet \times H_2O + (2-x)H_2O \quad (5)$$

Fig. 7 schematically depicts the formation of the mesoporous anatase TiO_2 spheres. The formation mechanisms of anatase nanocrystals and porous structure can be attributed to surface energy effects and Ostwald ripening, respectively. When the titanium glycolate precursor spheres are added to the sufficient hot water at a boiling temperature (~100 °C), the surface shell of the particles would contact the hot water at first as showed in step (a) in Fig. 7. According to the FTIR results, the incomplete hydrolysis precursor would undergo a further *in situ* hydrolysis and condensation on the surface layer firstly. The water also promotes the crystallization of amorphous TiO_2 [23]. Then, the fine anatase nanocrystal is

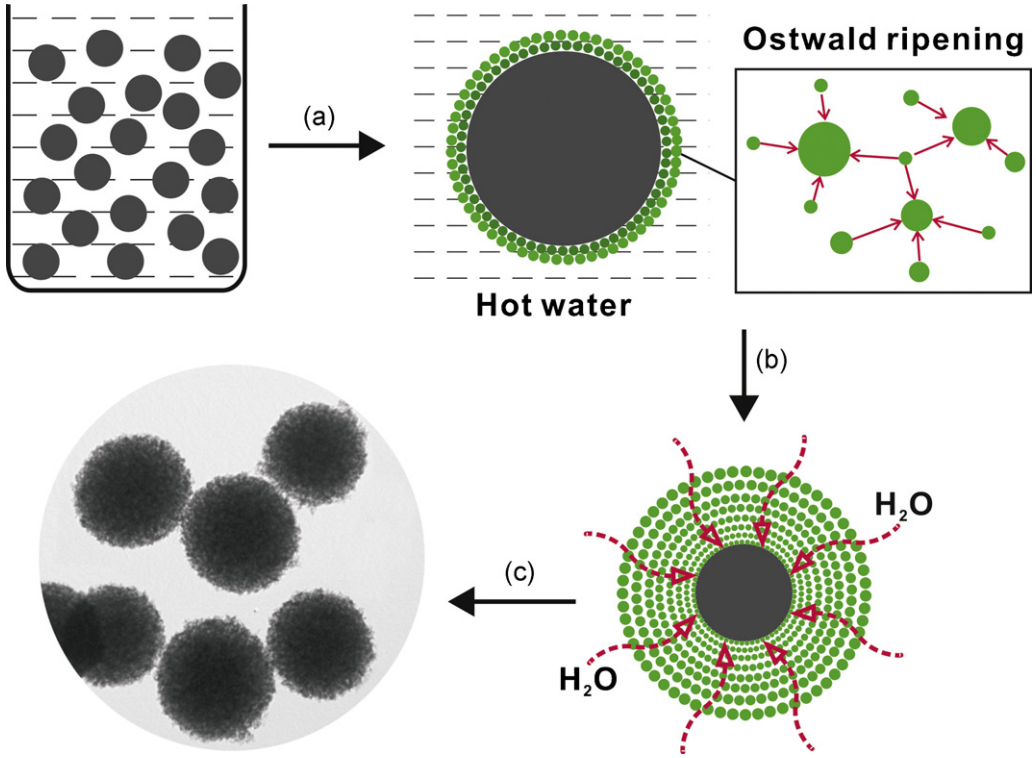

Fig. 7. Schematic process of the formation of mesoporous anatase TiO_2 spheres: (a) hot water surrounding the precursor sphere and surface becomes rough and get crystallization; (b) water further penetrates into the interior; (c) converts into mesoporous TiO_2 spheres completely.

formed due to the lower surface energy compared to other phases. The surface energy affects phase formation both in thermodynamics and in kinetics. Thermodynamically, if the nanoparticles are small enough, the anatase is the stable phase as a result of the lowest total energy. Based on the classical nucleation rate (J_N) formula (express as follow): [24]

$$J_N = J_0 \exp\left(\frac{-\Delta G^*}{RT}\right) = J_0 \exp\left(\frac{-16\pi V_m^2 \gamma^3}{3(RT)^3(\ln S)^2}\right) \quad (6)$$

where J_0 is a pre-factor determined by the frequency of collisions and reaction type, ΔG^* is the energy to form a critical nucleus, S is the supersaturation, and γ is the surface energy of the solid–liquid interface. Therefore, a lower surface energy significantly increases the nucleation kinetics, thus preferring to form anatase.

After nucleation, many small anatase crystals of different sizes form on the surface of sphere. According to Ostwald ripening theory [25,26], the smaller crystals slowly disappear and act as "nutrients" for the growth of bigger crystals due to the energetic factors, while the larger crystallites would serve as starting points (or nucleation seeds) on the outermost surface of spheres, so the voids gradually generate and the surface becomes rough. As the small grains get a further growth, some cracks form on the shell, making the hot water penetrate into the interior as showed in step (b) in Fig. 7. It is worth noting that the Ostwald ripening firstly takes place at the surface of compact spheres, which differs from the previous simpler outward ripening process [27]. With the inward ripening proceeding, the porous structure is further formed in the inner part of the spheres and the TiO_2 grains gradually grow into interconnected nano-cluster as showed in step (c) in Fig. 7. Finally, the anatase mesoporous spheres are formed. Interestingly, some brookite phase appears with the extension of reaction time, and this can also be attributed to the surface energy effect. It is known that the relative stability of TiO_2 polymorphs is size-dependent [28,29]. Anatase is most stable at sizes less than 11 nm while brookite between 11 nm and 35 nm. Besides, the transformation from anatase to brookite can be occurred at lower temperatures as a result of the low transformation activation energy (11.9 kJ mol^{-1}) [29]. Based on it, as the treatment time was increased, some grains get a further growth and exceed the critical size, thus forming the brookite nanocrystals.

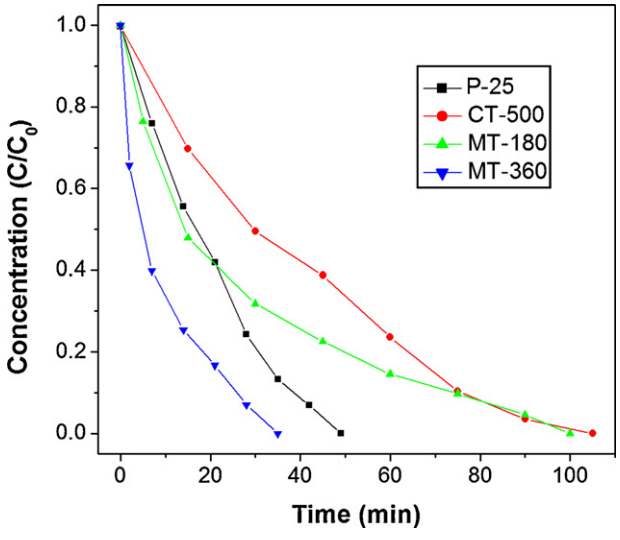

Fig. 8. Changes of RhB concentration in aqueous solution as a function of exposure time in the presence of P-25, CT-500, MT-180, and MT-360.

3.3. Photocatalytic properties

To study the photoactivity in degrading contaminants from water, four different TiO_2 catalysts (MT-180, MT-360, CT-500 and P-25) were used to investigate the photocatalytic degradation of RhB. The changes in RhB concentration during photocatalytic degradation are shown in Fig. 8. The results indicate that the mesoporous TiO_2 spheres MT-360 is able to completely degrade RhB within 35 min, showing the greatest photocatalytic activity of all. It is certain that the better property of the mesoporous titania spheres profits from two points: fast reactive rates thanks to the larger specific surface area of the mesoporous structure; higher reactive activity due to the anatase nanocrystals. Besides, P-25 exhibits better photocatalytic activity than MT-180 and CT-500 because of the biphase composite structures (anatase and brookite) and smaller particle size (30 nm).

4. Conclusions

A facile template-free method was developed to synthesize submicron-sized hierarchically mesoporous anatase TiO_2 spheres at low temperature by simply treating the titanium glycolate precursor with hot water. As the treatment time was increased, the porous structure and crystallinity of the particles were improved. The as-prepared mesoporous TiO_2 spheres consisted of interconnected nanosized anatase crystals show a large BET specific surface area (194.91 $m^2\ g^{-1}$), leading to the excellent adsorption capacity and better photocatalytic activity compared with P-25 photocatalyst. The formation mechanisms of porous structure and anatase nanocrystal are attributed to the Ostwald ripening and surface energy effects in the sufficient hydrolysis and condensation process of the precursor. This convenient strategy presents a new possibility for synthesis of porous anatase TiO_2 materials from an incomplete hydrolysis precursor. Furthermore, these sub-micron size powders can be easily separated and reused, thus showing a promising potential in environmental protection.

Acknowledgments

This work was partially supported by National Key Technology R&D Program of China (grant no. 2006BAJ05B05) and China Postdoctoral Science Foundation (grant no. 20080441245).

References

[1] B.O. Regan, M. Grätzel, Nature 353 (1991) 737.
[2] X.B. Chen, S.S. Mao, Chem. Rev. 107 (2007) 2891.
[3] W.A. Badawy, A.M. Fathi, R.M. El-Sherief, S.A. Fadl-Allah, J. Alloys Compd. 475 (2009) 911.
[4] Q.H. Shen, H. Yang, J.W. Gao, H.S. Ning, Z.Q. Cai, Chin. J. Inorg. Chem. 23 (2007) 1159.
[5] Y. Shen, J.C. Tao, F. Gu, L. Huang, J. Bao, J.C. Zhang, N. Dai, J. Alloys Compd. 474 (2009) 326.
[6] A. Rachel, M. Subrahmanyam, P. Boule, Appl. Catal. B: Environ. 37 (2002) 301.
[7] L.Z. Yang, L.Z. Zhu, C. Liu, M. Fang, G.H. Liu, X.B. Yu, Mater. Res. Bull. 43 (2008) 806.
[8] J.K. Liu, T.C. An, G.Y. Li, N.Z. Bao, G.Y. Sheng, J.M. Fu, Micropor. Mesopor. Mater. 124 (2009) 197.
[9] C.W. Wu, T. Ohsuna, M. Kuwabara, K. Kuroda, J. Am. Chem. Soc. 128 (2006) 4544.
[10] H.Y. Hao, J.L. Zhang, Mater. Lett. 63 (2009) 106.
[11] Q.H. Shen, H. Yang, J.W. Gao, J.G. Yang, Mater. Lett. 61 (2007) 4160.
[12] Z.Y. Zhang, F. Zuo, P.Y. Feng, J. Mater. Chem. 20 (2010) 2206.
[13] Q.H. Shen, Z.Q. Cai, J.W. Gao, H. Yang, Chin. J. Catal. 28 (2007) 153.
[14] V.F. Stone, R.J. Davis, Chem. Mater. 10 (1998) 1468.
[15] Y. Kotani, A. Matsuda, T. Kogure, M. Tatsumisago, T. Minami, Chem. Mater. 13 (2001) 2144.
[16] Y. Kotani, T. Matoda, A. Matsuda, T. Kogure, M. Tatsumisago, T. Minami, J. Mater. Chem. 11 (2001) 2045.
[17] S. Guo, Z.B. Wu, H.Q. Wang, F. Dong, Catal. Commun. 10 (2009) 1766.

[18] D.G. Kulkarni, A.V. Murugan, A.K. Viswanath, C.S. Gopinath, J. Nanosci. Nanotechnol. 9 (2009) 371.
[19] P. Raveendran, M. Eswaramoorthy, U. Bindu, M. Chatterjee, Y. Hakuta, H. Kawanami, F. Mizukami, J. Phys. Chem. C 112 (2008) 20007.
[20] X.C. Jiang, T. Herricks, Y.N. Xia, Adv. Mater. 15 (2003) 1205.
[21] K.S.W. Sing, D.H. Everett, R.A.W. Haul, L. Moscou, R.A. Pierotti, J. Rouquérol, T. Siemieniewska, Pure Appl. Chem. 57 (1985) 603.
[22] Z.Y. Yuan, B.L. Su, J. Mater. Chem. 16 (2006) 663.
[23] D. Reyes-Coronado, G. Rodríguez-Gattorno, M.E. Espinosa-Pesqueira, C. Cab, R. de Coss, G. Oskam, Nanotechnology 19 (2008) 145605.
[24] G. Oskam, J. Sol–gel Sci. Technol. 37 (2006) 161.
[25] W. Ostwald, Z. Phys. Chem. 22 (1897) 289.
[26] W. Ostwald, Z. Phys. Chem. 34 (1900) 495.
[27] H.G. Yang, H.C. Zeng, J. Phys. Chem. B 108 (2004) 3492.
[28] J.G. Li, T. Ishigaki, X.D. Sun, J. Phys. Chem. C 111 (2007) 4969.
[29] H.Z. Zhang, J.F. Banfield, J. Phys. Chem. B 104 (2000) 3481.